RSC Advances

COMMUNICATION

View Article Online
View Journal | View Issue

Vapour-based processing of hole-conductor-free $CH_3NH_3PbI_3$ perovskite/C_{60} fullerene planar solar cells†

Cite this: *RSC Adv.*, 2014, **4**, 28964

Received 26th April 2014
Accepted 17th June 2014

DOI: 10.1039/c4ra03820g

www.rsc.org/advances

Hao Hu,[ac] Dong Wang,[ac] Yuanyuan Zhou,[b] Jiliang Zhang,[d] Siliu Lv,[a] Shuping Pang,*[a] Xiao Chen,[a] Zhihong Liu,[a] Nitin P. Padture[b] and Guanglei Cui*[a]

A new sequential-vapour-deposition method is demonstrated for the growth of high-quality $CH_3NH_3PbI_3$ perovskite films. This has enabled the all-vapour, low-temperature fabrication of hole-conductor-free planar perovskite solar cells consisting of only a $CH_3NH_3PbI_3$/C_{60} bi-layer sandwiched between two electrical contacts, with a power conversion efficiency of 5.4%.

Organometallic trihalide perovskites with the general formula $(RNH_3)MeX_3$ (where R is an organic group, Me is Pb or Sn, and X is a halogen I, Br, or Cl) have recently emerged as new generation light harvesting materials in excitonic solar cells.[1–3] In particular, methylammonium (MA) lead triiodide ($CH_3NH_3PbI_3$ or $MAPbI_3$) has attracted great deal of attention since it was first applied as the light absorber in mesoscopic solar cells.[4–6] Within a short period of time the power conversion efficiency (PCE) of $MAPbI_3$-based solar cells has shot up dramatically to 16.2%.[4,6,7] This rapid rise in the performance is the result of the innate desirable properties of $MAPbI_3$, including favourable direct band gap, large adsorption coefficient, high carrier mobilities and long carrier (balanced) diffusion lengths.[1,5,6,8] With regards to the latter, Xing *et al.*[8] showed that the carrier diffusion length in solution-processed $MAPbI_3$ thin films is at least 100 nm, despite the non-ideal nature of the solution-spun $MAPbI_3$ films. Higher PCEs of ~12% were obtained by Malinkiewicz *et al.*[9] and Chen *et al.*[10] in planar (non-mesoscopic) solar cells based on better quality $MAPbI_3$ films of ~300 nm thickness. This suggests that maximizing the quality (coverage, crystallinity, texture) of $MAPbI_3$ films can lead to carriers diffusion lengths >300 nm, which is the key to realizing planar perovskite-based solar cells with high efficiencies.[8,9]

However, reliable deposition of high-quality films of phase-pure $MAPbI_3$ perovskites with full coverage and high crystallinity still remains a challenge.[5,6] One-step solution-spun $MAPbI_3$ generally results in films with pinholes due to high reaction rate between MAI and PbI_2.[4,10] To address this issue Burschka, *et al.*[4] developed a two-step method, where mesoporous TiO_2 is first infiltrated by solution-processed PbI_2, followed by dipping it in a MAI solution for the *in situ* formation of $MAPbI_3$. However, in the case of planar solar cells, where a mesoporous TiO_2 scaffold is not used, several hours are needed for the complete conversion of $MAPbI_3$, which can result in the peeling of the films.[4] In another study involving planar solar cells, the dipping process was replaced by extended annealing of the solution-processed PbI_2 film in a MAI-vapour-rich N_2 atmosphere at 150 °C.[10] However, this process may be not amenable to producing uniform $MAPbI_3$ films on organic substrates.[10] Meanwhile, Liu *et al.*[11] and Malinkiewicz *et al.*[9] used dual-source co-evaporation deposition to prepare uniform, pinhole-free films of $MAPbI_3$ or chorine-doped $MAPbI_3$, where the resulting planar solar cells delivered one of the highest PCEs. However, careful control of evaporation rates of the organic and the inorganic precursors is needed to achieve proper stoichiometry in the deposited films.

To that end, we demonstrate here a facile sequential-vapour-deposition (SVD) approach for the growth of high-quality $MAPbI_3$ films, which has enabled the fabrication of simple perovskite-based planar solar cells consisting of a $MAPbI_3$ perovskite/C_{60} fullerene bi-layer sandwiched between two electrical contacts (indium tin oxide (ITO) coated glass and thermally-evaporated Ag). A maximum PCE of 5.4% is achieved in these solar cells. To our knowledge, this type of bi-layer architecture, which is devoid of any additional blocking layer, any mesoporous scaffold (*e.g.* TiO_2, ZnO, or Al_2O_3), and any additional conducting organic layers, constitutes the simplest perovskite-based working solar cell reported thus far. Especially, while several groups have hole-conductor-free

[a]*Qingdao Institute of Bioenergy and Bioprocess Technology, Chinese Academy of Sciences, Qingdao 266101, P.R. China*

[b]*School of Engineering, Brown University, Providence, RI 02912, USA*

[c]*University of Chinese Academy of Sciences, Beijing 100049, P. R. China*

[d]*Department of Physics and Materials Science, City University of Hong Kong, SAR, Hong Kong*

† Electronic supplementary information (ESI) available. See DOI: 10.1039/c4ra03820g

mesoscopic perovskite solar cells, this is the first report of planar perovskite solar cells without use of hole conductors.

Fig. 1 is a schematic diagram of the SVD method for the growth of $MAPbI_3$ films. A nanostructured porous PbI_2 film is first vapour-deposited (Fig. 1A), followed by the vapour-deposition of MAI (Fig. 1B), which reacts *in situ* with the PbI_2 film (Fig. 1C). The freshly prepared $MAPbI_3$ film is further annealed at 100 °C for 30 min to produce a textured film (Fig. 1D). Note that strong texture in perovskite films have been suggested to be beneficial, most likely due to their improved carriers-transport properties.[12,13]

Detailed experimental procedures, including SVD growth of the films and solar cells fabrication, are presented in the accompanying (ESI†). Also presented in ESI are characterization procedures, including X-ray diffractometry (XRD), scanning electron microscopy (SEM), optical microscopy and ultraviolet-visible (UV-vis) optical spectroscopy, and procedures for solar cells testing.

Fig. 2 shows XRD patterns from the films at different stages of the SVD growth, and the evolution of the surface morphology of the thin films. The XRD pattern in Fig. 2A confirms the presence of layered PbI_2 (space group $P3m1$; $a = 4.600(2)$ Å, $b = 4.600(2)$ Å, $c = 6.9926(9)$ Å) in the film after the first step, and shows a strong 001 texture. The corresponding SEM image in Fig. 2B shows full-coverage, smooth film consisting of randomly-oriented packing of plate-like PbI_2. There is some amount of porosity between the adjacent PbI_2 plates in the film. The thickness of the PbI_2 plate-like structures is estimated at ~20–30 nm (see Fig. S1 in ESI†), which is responsible for the broadening of the XRD peaks in Fig. 2A. In contrast, solution-processed PbI_2 films prepared by spin-coating are relatively rough, with equiaxed grains of PbI_2 of few hundred nanometers size.[4] Fig. 2C is XRD pattern of PbI_2 film exposed to MAI vapour for 5 min, showing the presence of both PbI_2 and $MAPbI_3$. The corresponding SEM image in Fig. 2D shows features such as unreacted PbI_2 and pinholes. Visually, the side exposed to MAI vapour appears black ($MAPbI_3$), while the back side appears yellow (PbI_2) through the glass. This indicates that the PbI_2 + MAI → $MAPbI_3$ reaction is diffusion limited. After additional 10 min of MAI vapour exposure the reaction is complete, as confirmed by XRD (Fig. 2E); the XRD pattern shows phase-pure tetragonal $MAPbI_3$ (space group $I4/mcm$; $a = b = 8.8745(7)$ Å, $c = 12.665(2)$ Å) and the absence of PbI_2. The corresponding SEM image (Fig. 2F) shows a uniform, smooth film of polycrystalline $MAPbI_3$ with a grain size of ~500 nm. The entire thickness

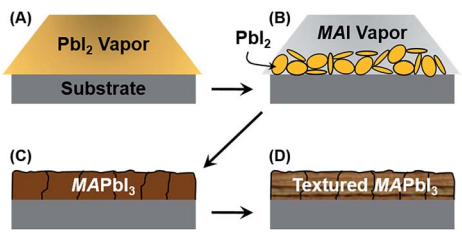

Fig. 1 Schematic representation of the sequential-vapour deposition (SVD) process for the growth of $MAPbI_3$ perovskite films.

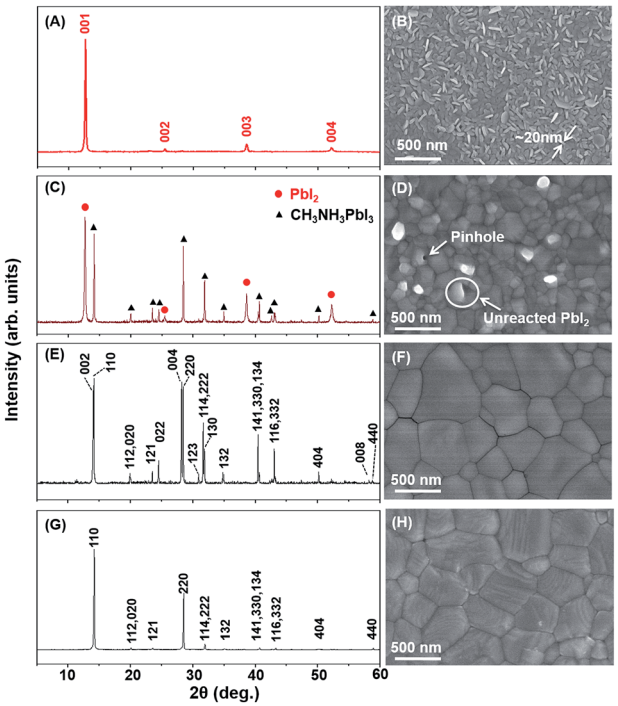

Fig. 2 Indexed XRD patterns and corresponding SEM images (top surface) of films at the different stages during SVD growth: (A and B) after PbI_2 vapour deposition; (C and D) partially reacted with MAI vapour (5 min); (E and F) fully reacted with MAI vapour (15 min); (G and H) after annealing at 100 °C for 30 min.

(~350 nm) of the $MAPbI_3$ film appears dark visually. Heat-treatment (100 °C, 30 min.) of the $MAPbI_3$ perovskite film results in the development of strong 110 texture (Fig. 2G), and a slightly distorted structure ($a = 8.876(5)$, $b = 8356(2)$ Å, $c = 12.530(6)$ Å). SEM image in Fig. 2H shows no grain coarsening as a result of the heat-treatment, but shows faceting of the individual grains. How this texture develops during this modest heat-treatment is not know at this time.

It appears that the nanoporous nature of the vapour-deposited PbI_2 film (Fig. 2B), with its large specific surface area, allows easy ingress and contact with MAI vapour, promoting rapid and more uniform reaction between PbI_2 and MAI. This results in phase-pure $MAPbI_3$ films that are pinhole-free, uniform, and smooth (Fig. 2F). Since the film thickness is ~350 nm, and the size of the $MAPbI_3$ grains is ~500 nm, most of the $MAPbI_3$ grains span the entire thickness of the film. In other words, majority of the grain boundaries in the SVD-processed $MAPbI_3$ films are expected to run vertically between the substrate and the film surface, and that the horizontal grain boundaries across the path of carriers transport are likely to be in the minority.

Fig. 3A shows the UV-vis absorbance spectrum of the $MAPbI_3$ perovskite film (on ITO) prepared by the SVD method and the corresponding differential transmission ($\Delta T/T$) spectrum (inset is an optical photograph showing dark-colored film). The $CH_3NH_3PbI_3$ perovskite film exhibits strong adsorption of UV-vis light up to ~790 nm wavelength, which is consistent with what is reported in the literature.[8,14,15] However, from the

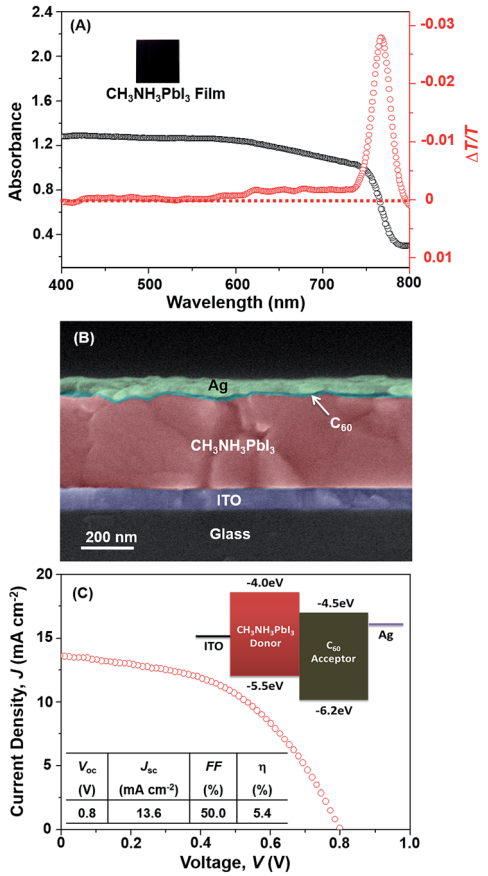

Fig. 3 (A) UV-vis absorption spectrum and transformed differential transmission spectrum of $MAPbI_3$ perovskite film (inset: optical photograph). (B) Cross-sectional SEM image of a $MAPbI_3/C_{60}$ solar cell (false color). (C) Current density (J) – voltage (V) response of a $MAPbI_3/C_{60}$ solar cell under AM1.5G one sun illumination (top inset: energy-levels diagram; bottom inset: extracted solar cell performance parameters).

differential transmission spectrum, the SVD-processed $CH_3NH_3PbI_3$ perovskite film shows only one intense photobleaching peak at ~760 nm which is assigned to the direct band gap transition. The broad photobleaching peak at ~480 nm, which is typically observed in $MAPbI_3$ perovskite films, is virtually absent in the $\Delta T/T$ spectrum in Fig. 3A. This is probably related to unique band structure in the SVD-processed $MAPbI_3$ perovskite films that exhibits unique crystal morphology. These distinct UV-vis absorption characteristics of the SVD-processed $MAPbI_3$ perovskite films also indicate the likelihood of an efficient photo-induced charge transfer during the solar cell operation.[16]

Fig. 3B is a color-enhanced cross-sectional SEM image of a typical $MAPbI_3/C_{60}$ bilayer solar cell fabricated in this study, illustrating the simple cell architecture. All three layers—$MAPbI_3$, C_{60}, Ag—are vapour deposited (see ESI†). The energy-levels diagram of this simple cell architecture is shown in the Fig. 3C inset. Here the $MAPbI_3$ film serves as absorber, electron-donor, hole-conductor, and electron-blocking layer. Whereas the C_{60} layer serves as electron-acceptor, electron-conductor, and hole-blocking layer. Since $MAPbI_3$ is a good hole-conductor, additional hole-conducting layers typically used in perovskite-based solar cells can be eliminated while retaining high PCEs.[17–19] Furthermore, the widely used mesoporous TiO_2 electron-acceptor/-conductor scaffold and/or dense TiO_2 hole-blocking layer, which require high-temperature processing, have been eliminated in these solar cells.[17–19] Efficient electron-hole dissociation occurs at the $MAPbI_3/C_{60}$ interface, making C_{60} a promising candidate as a non-oxide electron-acceptor/-conductor and hole-blocking layer in perovskite-based solar cells.[14,15]

Fig. 3C shows a typical current density (J) – voltage (V) response of the $MAPbI_3/C_{60}$ bilayer solar cell under AM1.5G simulated one sun illumination, and the solar-cell performance parameters are reported in the inset. Ten solar cells were tested, and their performance data are summarized in Table S1 (see ESI†), with the PCE ranging from 4.1% to 5.4%. Considering the simplicity of these solar cells, a maximum PCE of 5.4%, an open-circuit voltage (V_{OC}) of 0.8 V, and a short circuit current density (J_{SC}) of 13.6 mA cm^{-2}, are promising, and they can be attributed to the high quality of the SVD-processed $MAPbI_3$ films. The estimate of the maximum V_{OC} is given by:[14]

$$V_{OC} = \left(\left[E^{HOMO}_{Donor} \right] - \left[E^{LUMO}_{Acceptor} \right] \right) / e \quad (1)$$

Substituting the values from the energy-levels diagram in Fig. 3C (inset) in eqn (1), the maximum V_{OC} is estimated at 1.0 V for the $MAPbI_3/C_{60}$ heterojunction, representing a 20% loss in the measured V_{OC} (0.8 V) in the $MAPbI_3/C_{60}$ bi-layer solar cell (Fig. 3C).

Jeng *et al.*[14] and Chiang *et al.*[20] report PCEs of 1.6% and 3.62%, respectively, for solution-processed $MAPbI_3/C_{60}$ solar cells, but their solar cells also contain additional layers of poly(3,4-ehylenedioxythiophene) poly(styrene-sulfonated) (PEDOT:PSS) and bathocuproine (BCP). The PEDOT:PSS layer is the hole transporter and it appears necessary for one-step solution processing of $MAPbI_3$,[18] and the BCP layer is used as a hole-blocker. The voltage loss in $MAPbI_3/C_{60}$ solar cells by Jeng *et al.*[17] is 45%, whereas cells by Chiang *et al.*[10] show a lower loss of 16%. The use of a layer of a C_{60} derivate—(6,6)-phenyl-C_{61}-butyric acid methyl ester ($PC_{61}BM$)—instead of the C_{60} layer, in solution-processed $MAPbI_3/PC_{61}BM$ solar cells results in higher PCE (7.4%),[18] however, those cells also use the additional layer of PEDOT:PSS. The maximum estimated V_{OC} for these $MAPbI_3/PC_{61}BM$ is 1.23 V, and the measured V_{OC} in those cells is 0.91 V (ref. 18) or a 26% loss. Thus, the voltage loss in the simple $MAPbI_3/C_{60}$ bi-layer solar reported here is one of the lowest for solar cells based on $MAPbI_3$/fullerene heterojunctions, which is attributed to the improved coverage of perovskite film by SVD method.

With regard to J_{SC}, the measured value of 13.6 mA cm^{-2} reported here is the highest among all the $MAPbI_3$/fullerene heterojunction solar cells reported so far.[14,15,20] This is attributed to the relatively thicker and denser SVD-processed $MAPbI_3$ films used here that are able to absorb light more efficiently. The fill factor (FF) of 50% is relatively low in these $MAPbI_3/C_{60}$ solar cells, which could be due to various factors, including non-

ideal electrical contacts. Thus, there is plenty of room for improvement in this regard through further optimization of the ITO surface and the C_{60}/Ag interface.

Conclusions

An SVD method is demonstrated for the growth of high-quality $MAPbI_3$ films, and the possible growth mechanisms are elucidated. This constitutes a new contribution to the menu of processing methods available for the growth of $MAPbI_3$ perovskite films. The resulting $MAPbI_3$ films are pinhole-free, uniform and smooth, and most of the textured $MAPbI_3$ grains within the films span the entire thickness of the film. The high quality of the $MAPbI_3$ films allowed us to fabricate hole-conductor-free planar $MAPbI_3$ perovskite solar cells at low temperature (100 °C maximum) that deliver a promising PCE of 5.4% with V_{OC} of 0.8 V. While the simple bi-layer cell architecture is used here to demonstrate the efficacy of the SVD process, high-quality $MAPbI_3$ films grown by the SVD process can be used in more complex solar cell architectures for much higher performance, and also in other future optoelectronic devices.

Acknowledgements

This research was funded by the Chinese National Natural Science Foundation (grant no. 51202266), Natural Science Foundation of Shandong Province (ZR2013FZ001), the Research Program of Qingdao (13-1-4-228-jch, 12-1-4-9-(4)-jch, 12-4-1-24-gx) and the U.S. National Science Foundation (grant no. DMR-1305913).

Notes and references

1 G. Hodes, *Science*, 2013, **342**, 317–318.
2 B. V. Lotsch, *Angew. Chem., Int. Ed.*, 2014, **53**, 635–637.
3 S. Kazim, M. K. Nazeeruddin, M. Grätzel and S. Ahmad, *Angew. Chem., Int. Ed.*, 2014, **53**, 2812–2824.
4 J. Burschka, N. Pellet, S. J. Moon, R. Humphry-Baker, P. Gao, M. K. Nazeeruddin and M. Gratzel, *Nature*, 2013, **499**, 316–319.
5 N. G. Park, *J. Phys. Chem. Lett.*, 2013, **4**, 2423–2429.
6 H. S. Kim, S. H. Im and N. G. Park, *J. Phys. Chem. C*, 2014, **118**, 5615–5625.
7 A. Kojima, K. Teshima, Y. Shirai and T. Miyasaka, *J. Am. Chem. Soc.*, 2009, **131**, 6050–6051.
8 G. C. Xing, N. Mathews, S. Y. Sun, S. S. Lim, Y. M. Lam, M. Grätzel, S. Mhaisalkar and T. C. Sum, *Science*, 2013, **342**, 344–347.
9 O. Malinkiewicz, A. Yella, Y. H. Lee, G. M. Espallargas, M. Grätzel, M. K. Nazeeruddin and H. J. Bolink, *Nat. Photonics*, 2014, **8**, 128–132.
10 Q. Chen, H. Zhou, Z. Hong, S. Luo, H. S. Duan, H. H. Wang, Y. Liu, G. Li and Y. Yang, *J. Am. Chem. Soc.*, 2014, **136**, 622–625.
11 M. Liu, M. B. Johnston and H. J. Snaith, *Nature*, 2013, **501**, 395–398.
12 J. M. Ball, M. M. Lee, A. Hey and H. J. Snaith, *Energy Environ. Sci.*, 2013, **6**, 1739–1743.
13 E. Edri, S. Kirmayer, A. Henning, S. Mukhopadhyay, K. Gartsman, Y. Rosenwaks, G. Hodes and D. Cahen, *Nano Lett.*, 2014, **14**, 1000–1004.
14 S. Y. Sun, T. Salim, N. Mathews, M. Duchamp, C. Boothroyd, G. C. Xing, T. C. Sum and Y. M. Lam, *Energy Environ. Sci.*, 2014, **7**, 399–407.
15 J. Y. Jeng, Y. F. Chiang, M. H. Lee, S. R. Peng, T. F. Guo, P. Chen and T. C. Wen, *Adv. Mater.*, 2013, **25**, 3727–3732.
16 A. Marchioro, J. Teuscher, D. Friedrich, M. Kunst, R. Krol, T. Moehl, M. Grätzel and J. E. Moser, *Nat. Photonics*, 2014, **8**, 250–255.
17 L. Etgar, P. Gao, Z. S. Xue, Q. Peng, A. K. Chandiran, B. Liu, M. K. Nazeeruddin and M. Grätzel, *J. Am. Chem. Soc.*, 2012, **134**, 17396–17399.
18 W. Abu Laban and L. Etgar, *Energy Environ. Sci.*, 2013, **6**, 3249–3253.
19 J. Shi, J. Dong, S. Lv, Y. Xu, L. Zhu, J. Xiao, X. Xu, H. Wu, D. Li, Y. Luo and Q. Meng, *Appl. Phys. Lett.*, 2014, **104**, 063901.
20 Y. F. Chiang, J. Y. Jeng, M. H. Lee, S. R. Peng, P. Chen, T. F. Guo, T. C. Wen, Y. J. Hsu and C. M. Hsu, *Phys. Chem. Chem. Phys.*, 2014, **16**, 6033–6040.